10.1071/CH18512_AC

Australian Journal of Chemistry 2019, 72(4), 288-294

Supplementary Material

Effect of Rhenium(I) Complexation on Aza-Michael Additions to 5-Amino-1,10-Phenanthroline with [^{18}F]Ethenesulfonyl Fluoride towards PET-Optical Tracer Development

Mitchell A. Klenner,[A,B,F] *Giancarlo Pascali,*[A,C,F] *Bo Zhang,*[A,D] *Gianluca Ciancaleoni,*[E] *Massimiliano Massi,*[B] *and Benjamin H. Fraser*[A]

[A]Human Health, Australian Nuclear Science and Technology Organisation (ANSTO), Lucas Heights, NSW 2229, Australia.

[B]Department of Chemistry, Curtin University, Bentley, WA 6102, Australia.

[C]Brain and Mind Centre, University of Sydney, Sydney, NSW 2050, Australia.

[D]School of Chemistry, Monash University, Melbourne, Vic. 3800, Australia.

[E]Dipartimento di Chimica e Chimica Industriale Università di Pisa, Pisa 56127, Italy.

[F]Corresponding authors. Email: mitchk@ansto.gov.au; gianp@ansto.gov.au

Contents

S1. NMR spectra of precursors and standards

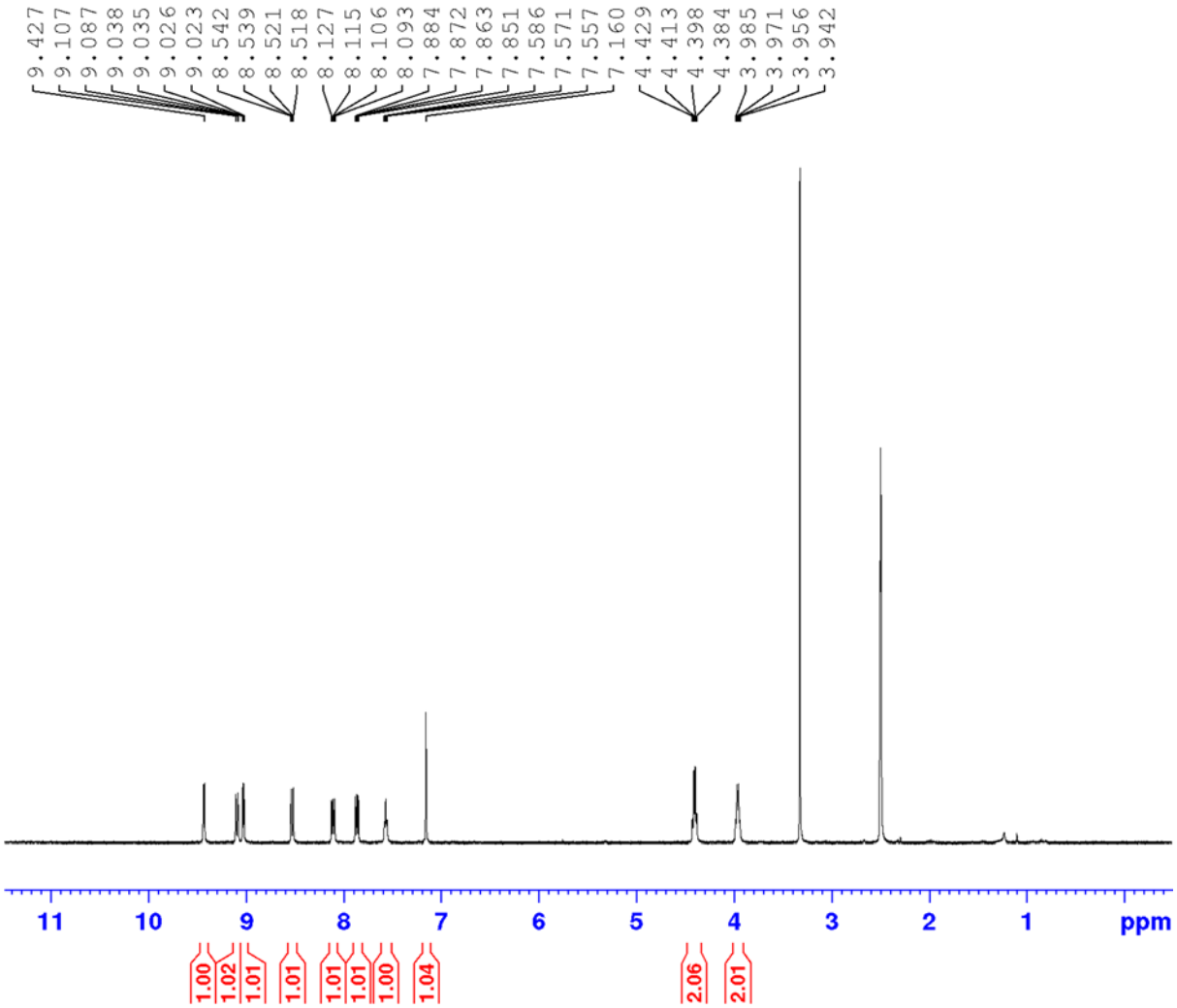

Figure S1.1. 1H-NMR spectrum of **RePhenESF** in DMSO-d_6 showing the expected peak area integration for twelve protons.

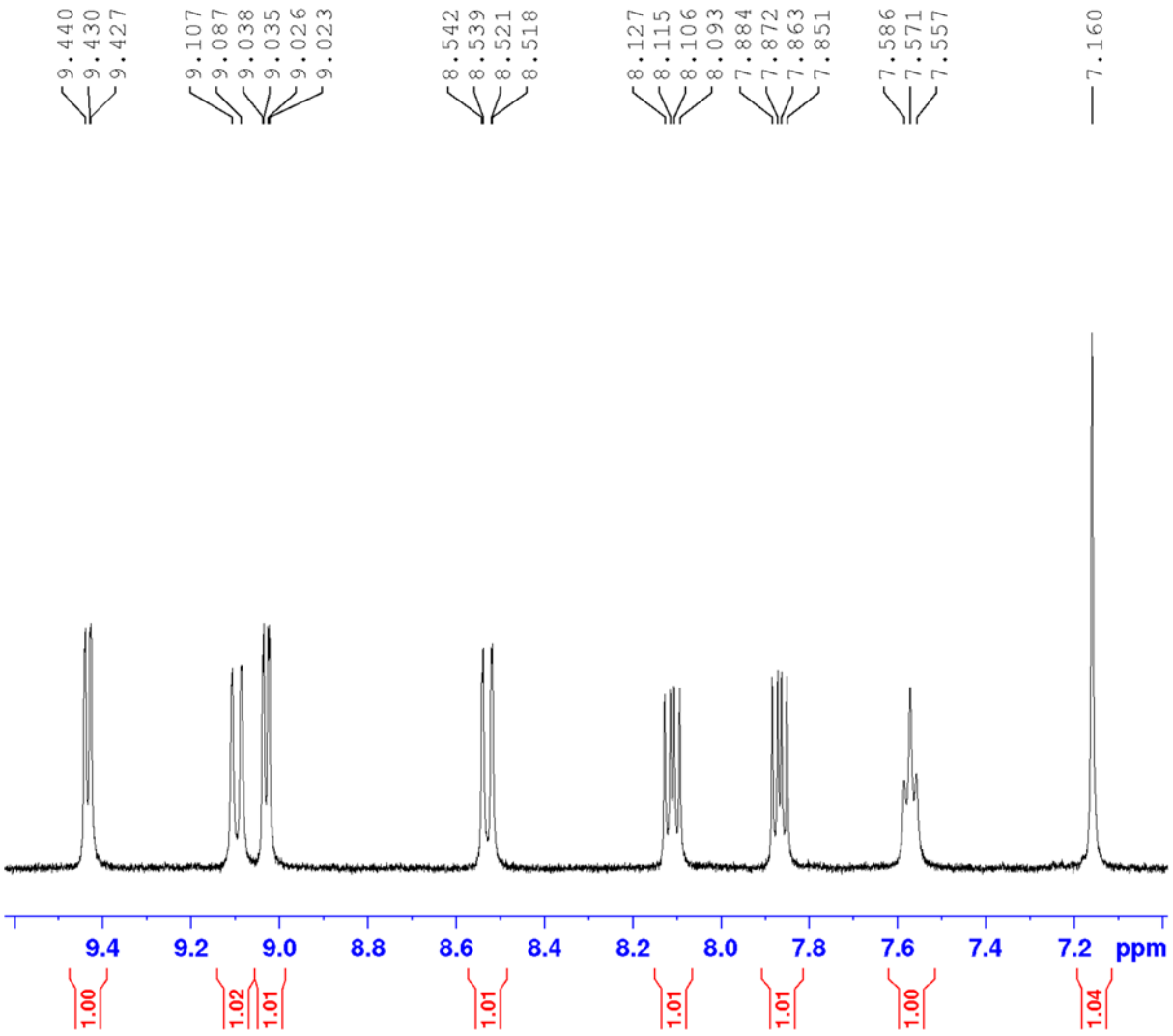

Figure S1.2. Zoomed in view of the aromatic region within the ^{1}H-NMR spectrum of **RePhenESF** in DMSO-d$_6$.

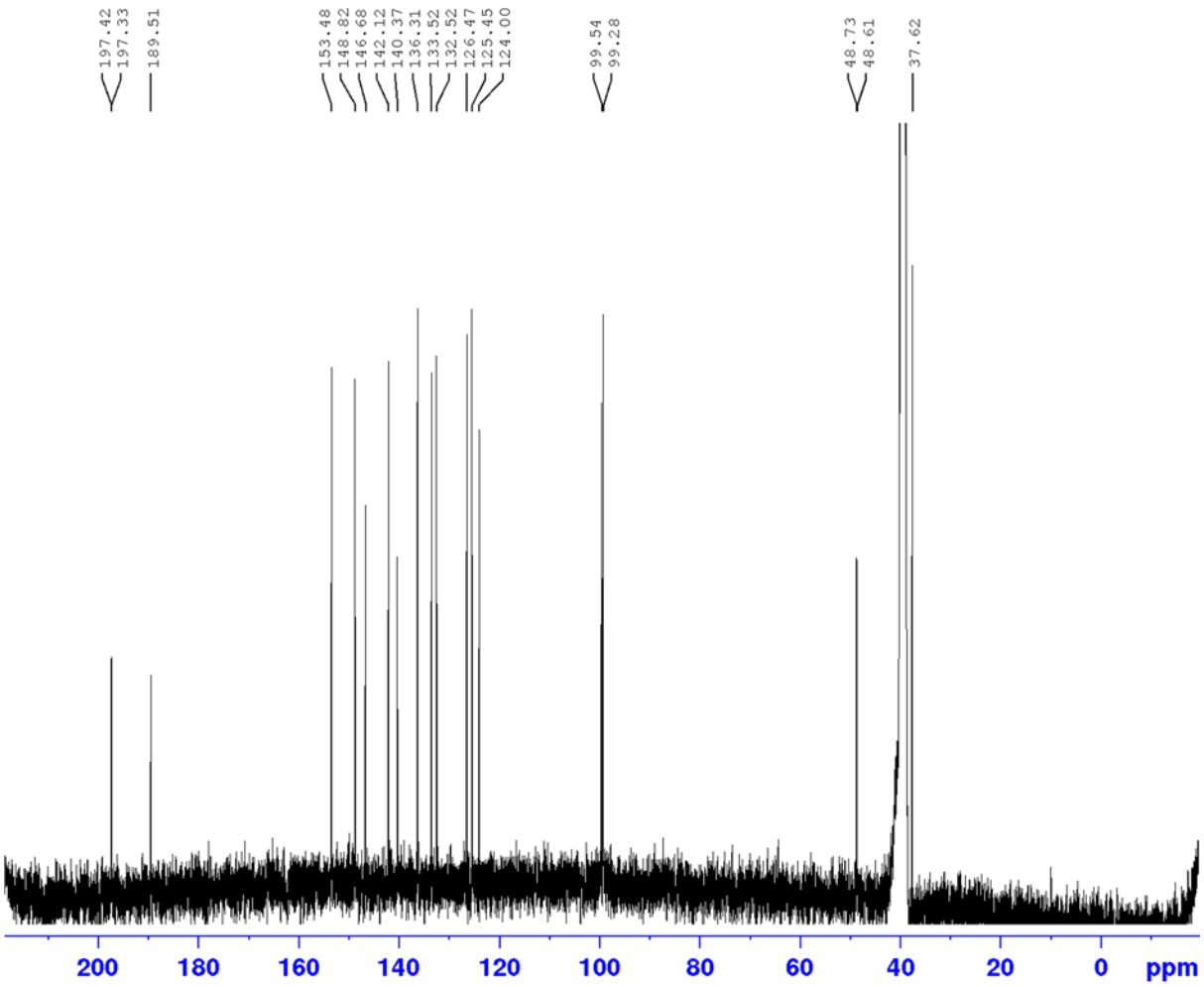

Figure S1.3. ^{13}C-NMR spectrum of **RePhenESF** in DMSO-d_6 exhibiting the expected three downfield shifted tricarbonyl signals at >180 ppm and fluorine splitting patterns.

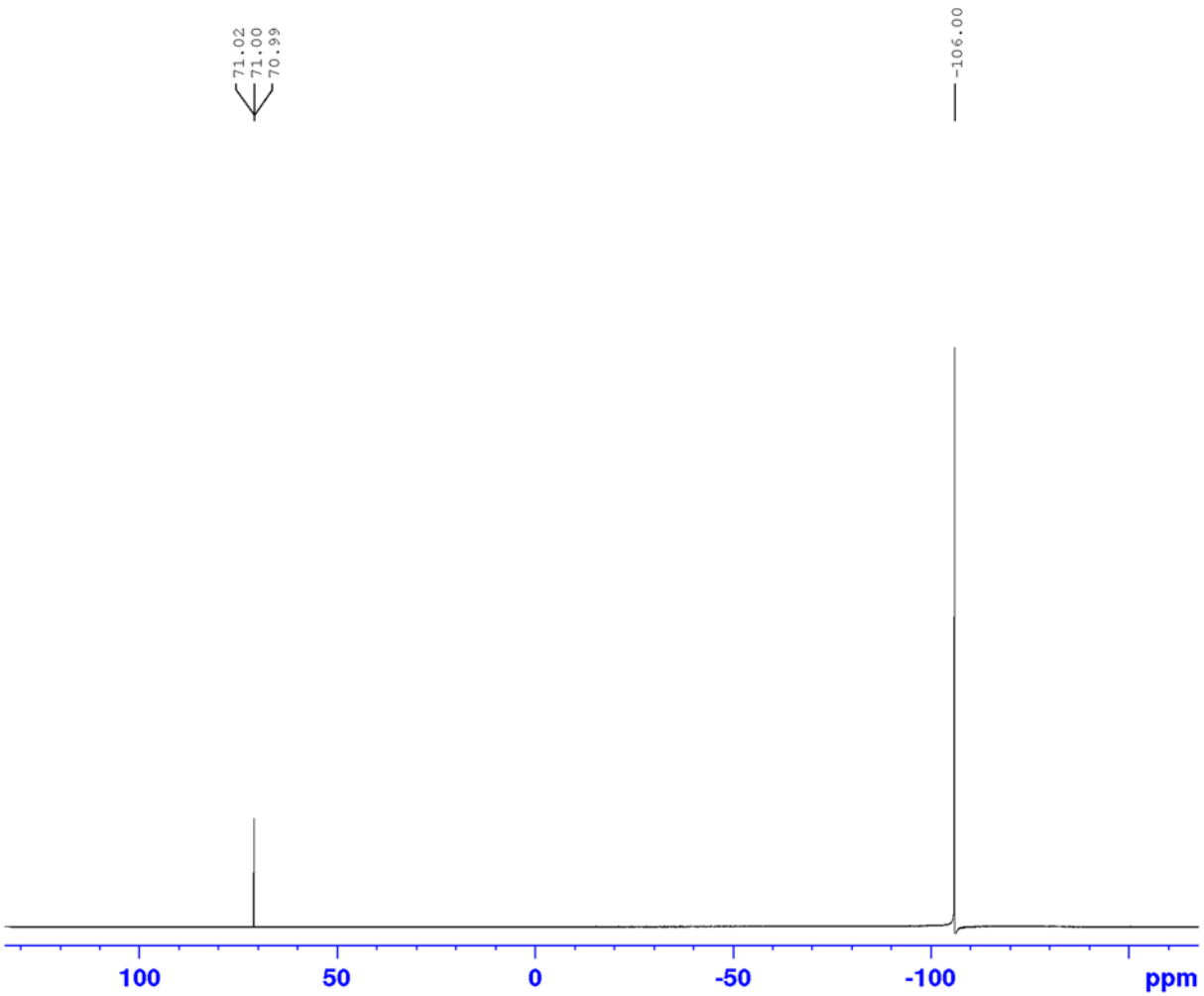

Figure S1.4. ^{19}F-NMR of **RePhenESF** exhibiting the fluorine-19 signal at *approx.* 71 ppm and the *para*-difluorobenzene fluorine-19 signal at -106 ppm (used as a calibrating standard).

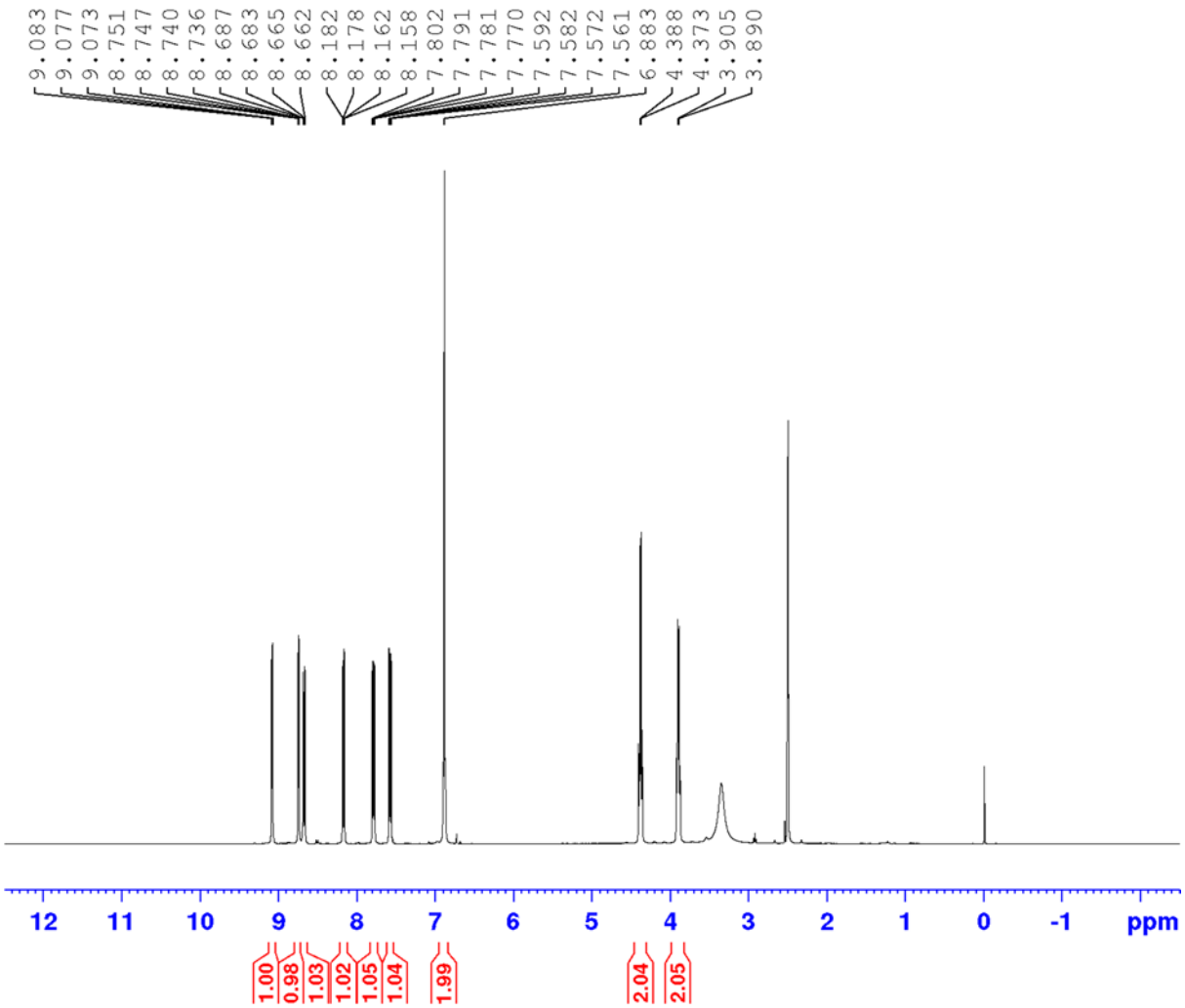

Figure S1.5. 1H-NMR spectrum of **PhenESF** in DMSO-d_6 showing the expected peak area integration for twelve protons as shifted upfield with respect to **RePhenESF**.

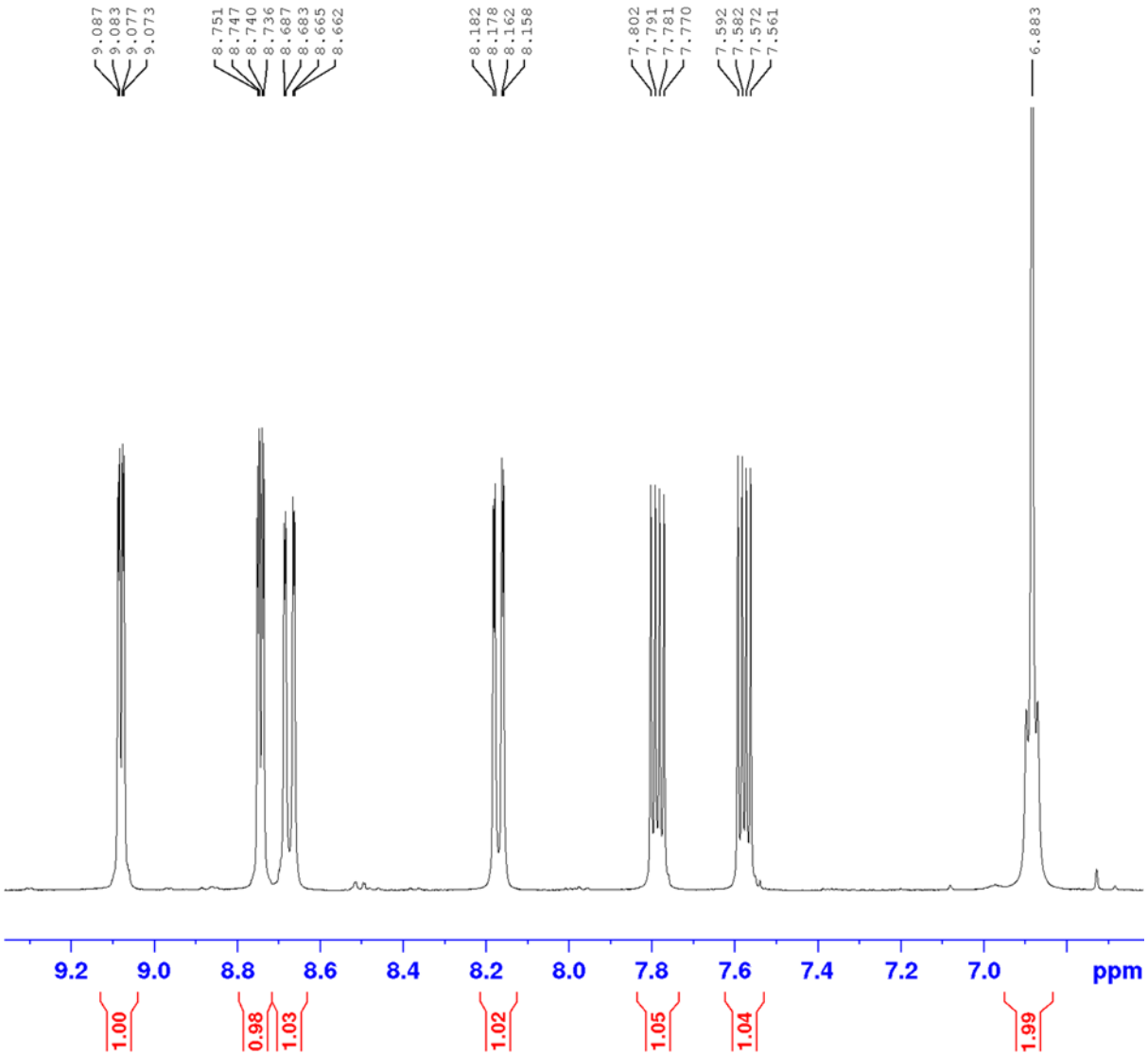

Figure S1.6. Zoomed in view of the eight aromatic protons within the ^{1}H-NMR spectrum of **PhenESF** in DMSO-d$_6$.

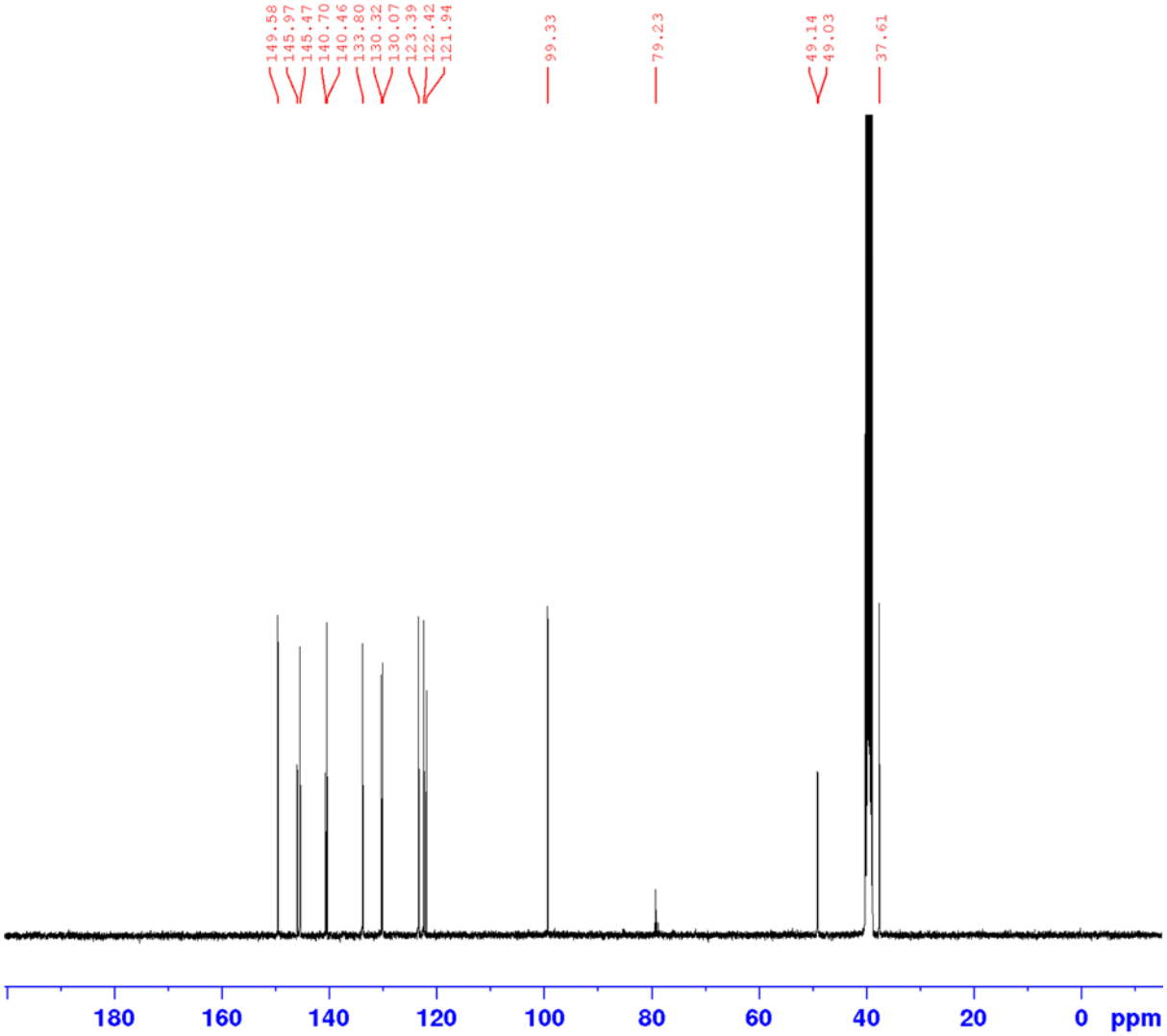

Figure S1.7. ^{13}C-NMR spectrum of **PhenESF** in DMSO-d_6 showing the expected sixteen carbon signals (twelve from the phenanthroline ring and four from fluorine splitting of the two carbon atoms within the ethylsulfonyl fluoride group).

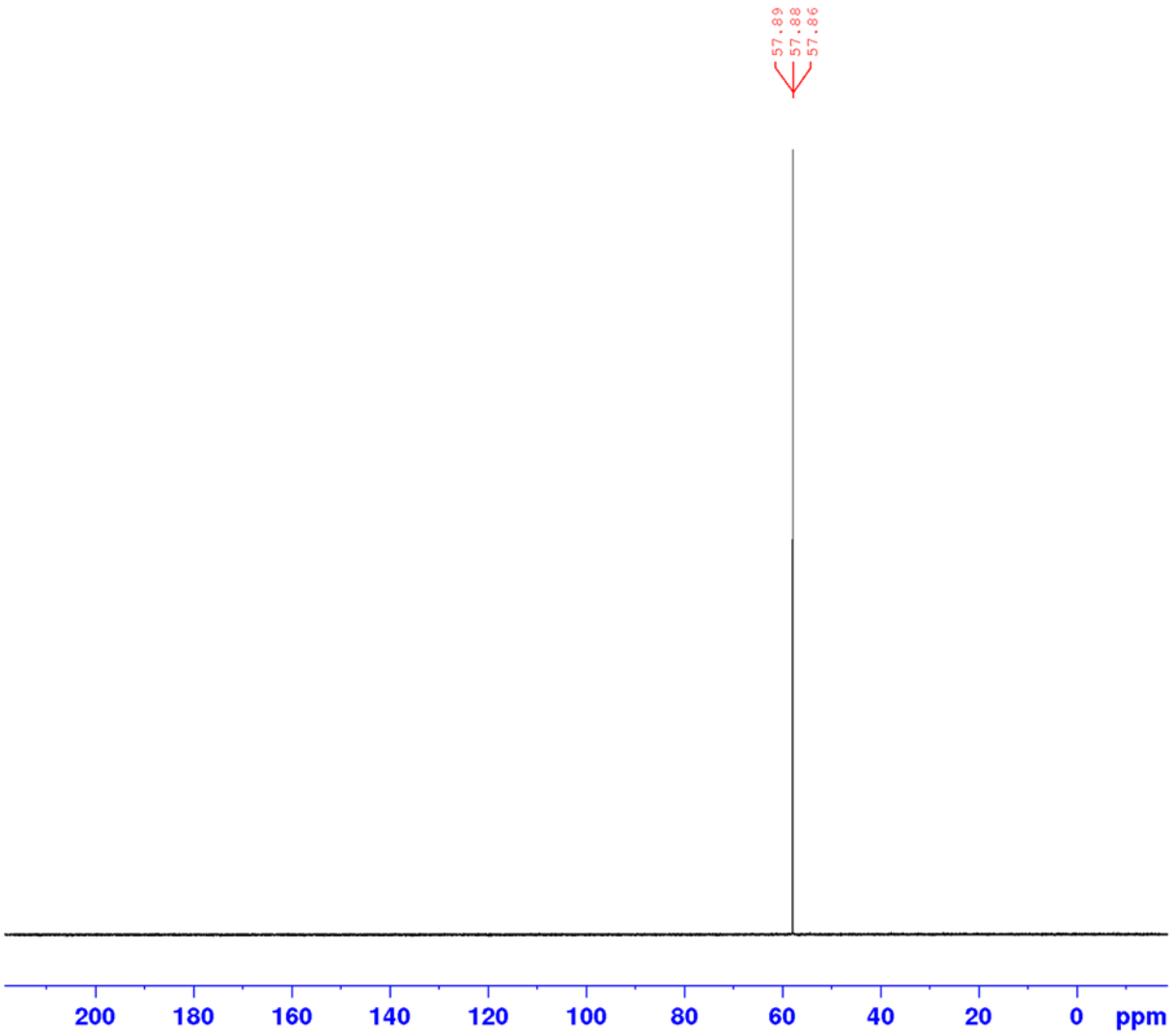

Figure S1.8. ^{19}F-NMR of **PhenESF** exhibiting the fluorine-19 signal at *approx.* 58 ppm.

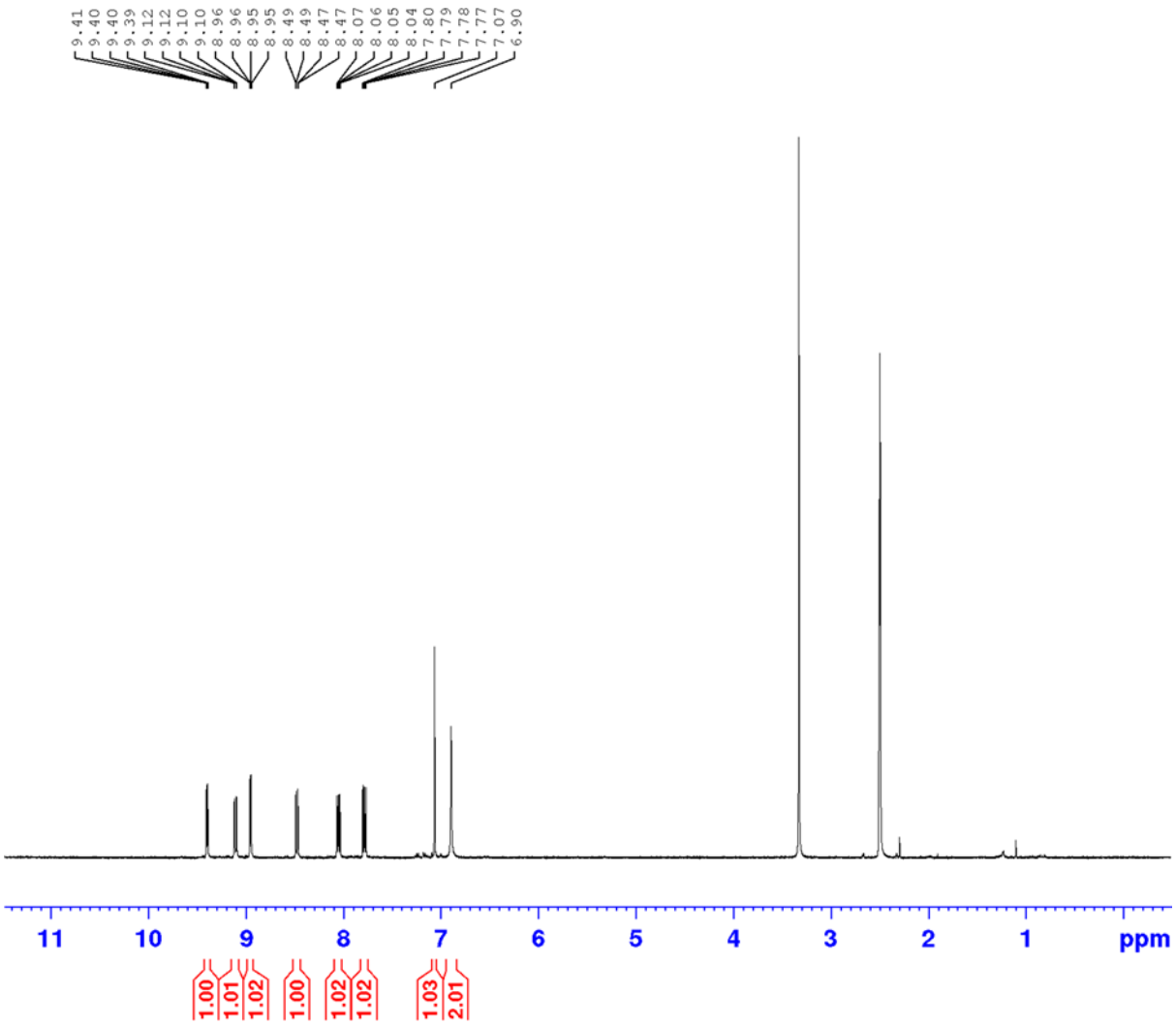

Figure S1.9. 1H-NMR spectrum of **RePhenNH2** in DMSO-d_6 showing the expected peak area integration for nine protons.

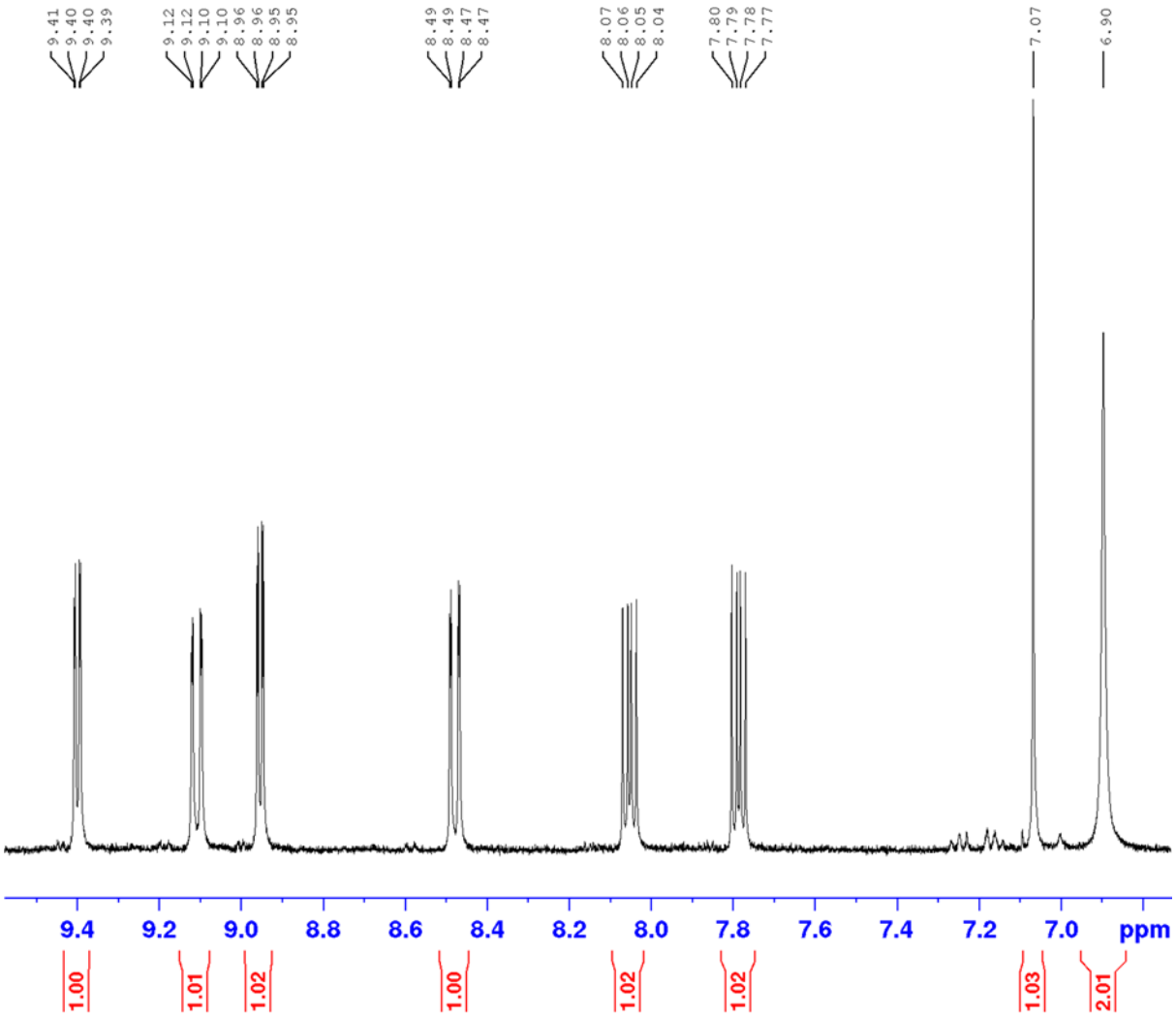

Figure S1.10. Zoomed in region of the nine aromatic protons in the 1H-NMR spectrum of **RePhenNH2** in DMSO-d_6.

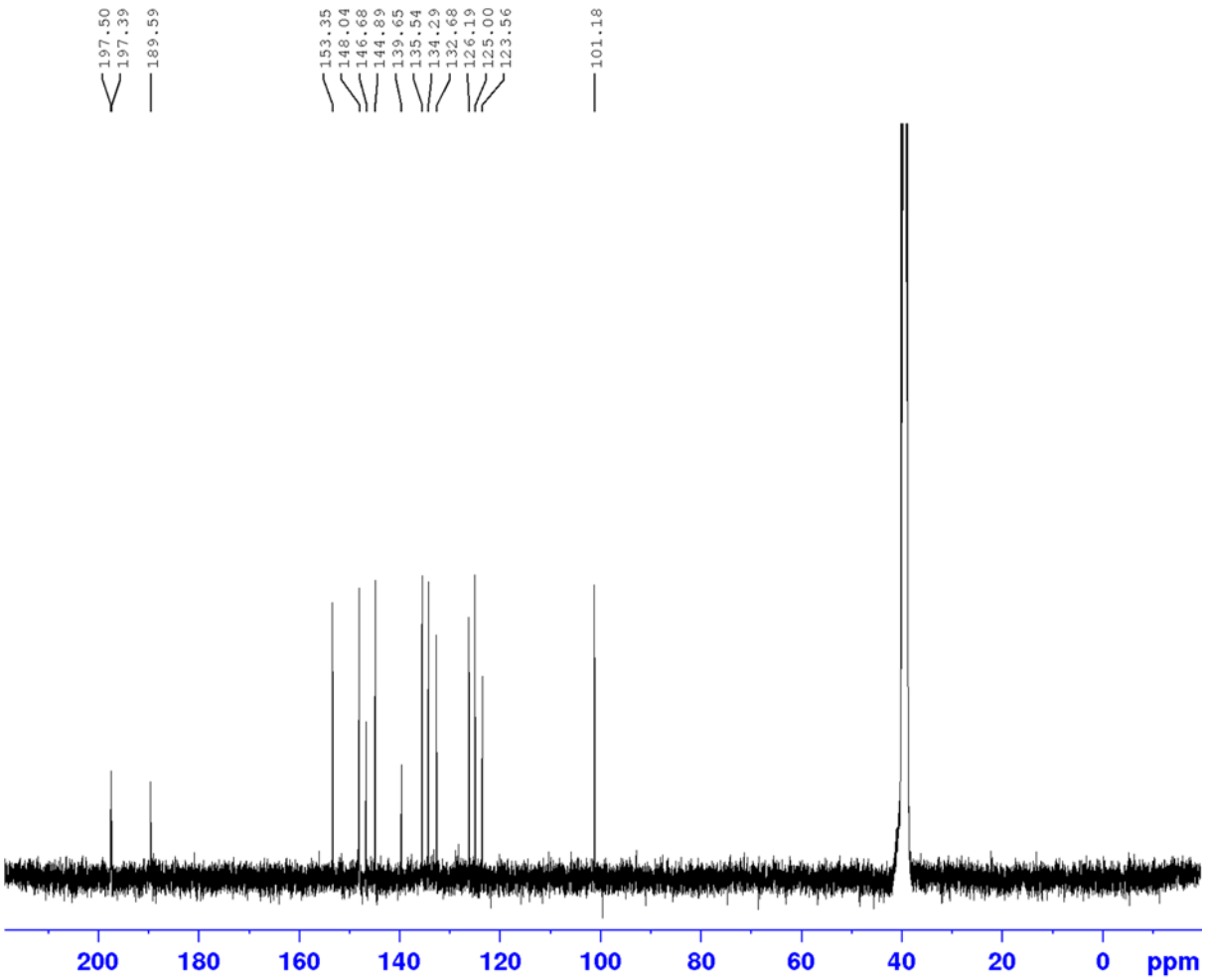

Figure S1.11. ^{13}C-NMR spectrum of **RePhenNH$_2$** in DMSO-d$_6$ showing the expected fifteen carbon signals, including the three at >180ppm corresponding to the tricarbonyl carbon nuclei.

S2. FTIR Spectra of rhenium(I) complexes

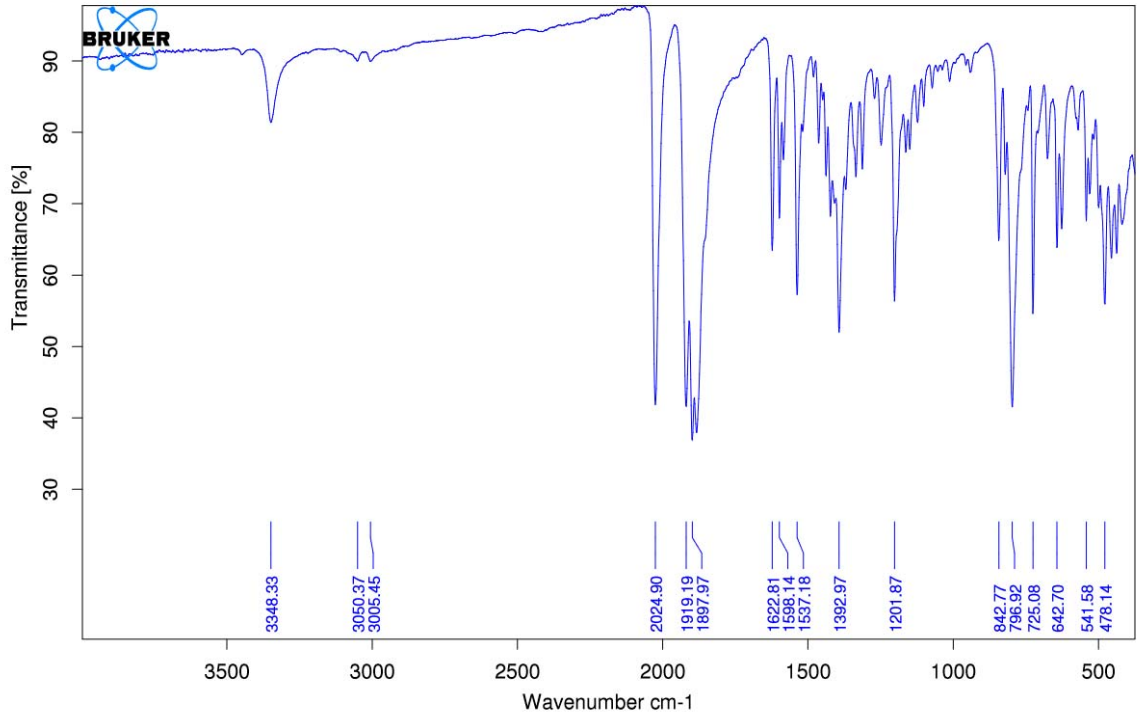

Figure S2.1. FTIR spectrum of **RePhenESF**.

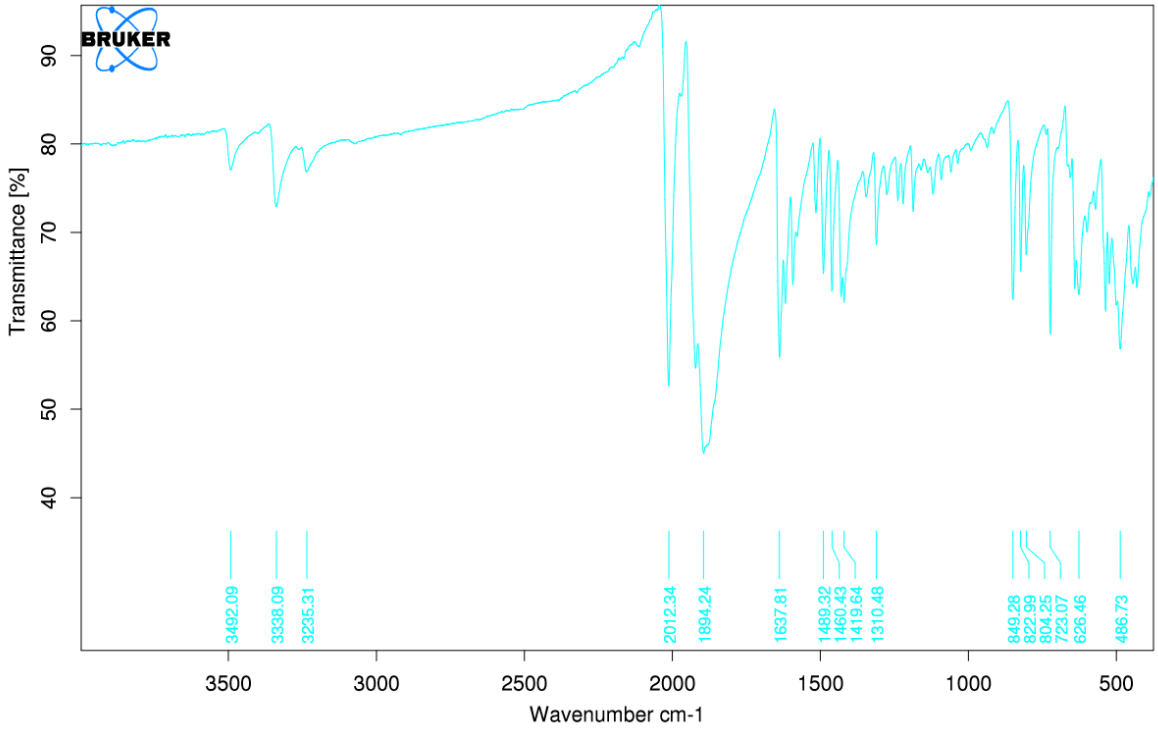

Figure S2.12. FTIR spectrum of **RePhenNH$_2$**.

S3. RadioTLC results for RCY verification

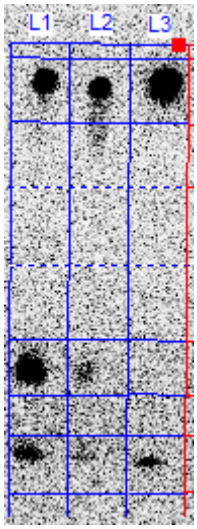

Figure S3.1. Sampled radioTLC results for the radiosyntheses of **[^{18}F]PhenESF** (70°C left, 40°C middle) and **[^{18}F]RePhenESF** (40°C right) used to validate RCYs attained by non-isolated radioHPLC peak integrations.

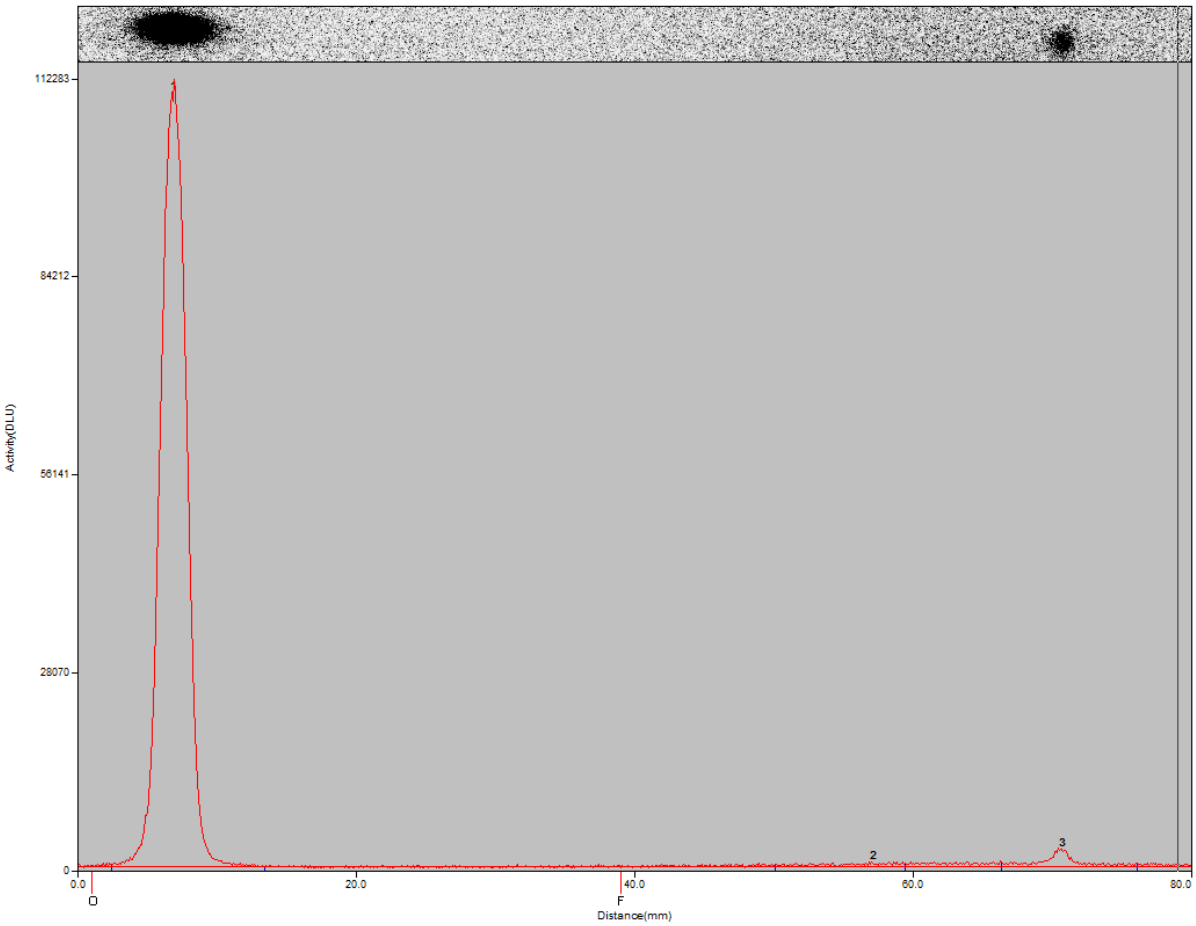

Figure S3.2. RadioTLC peak integration for reaction forming **[^{18}F]RePhenESF** at 40°C in 3% RCY (2% by radioHPLC).

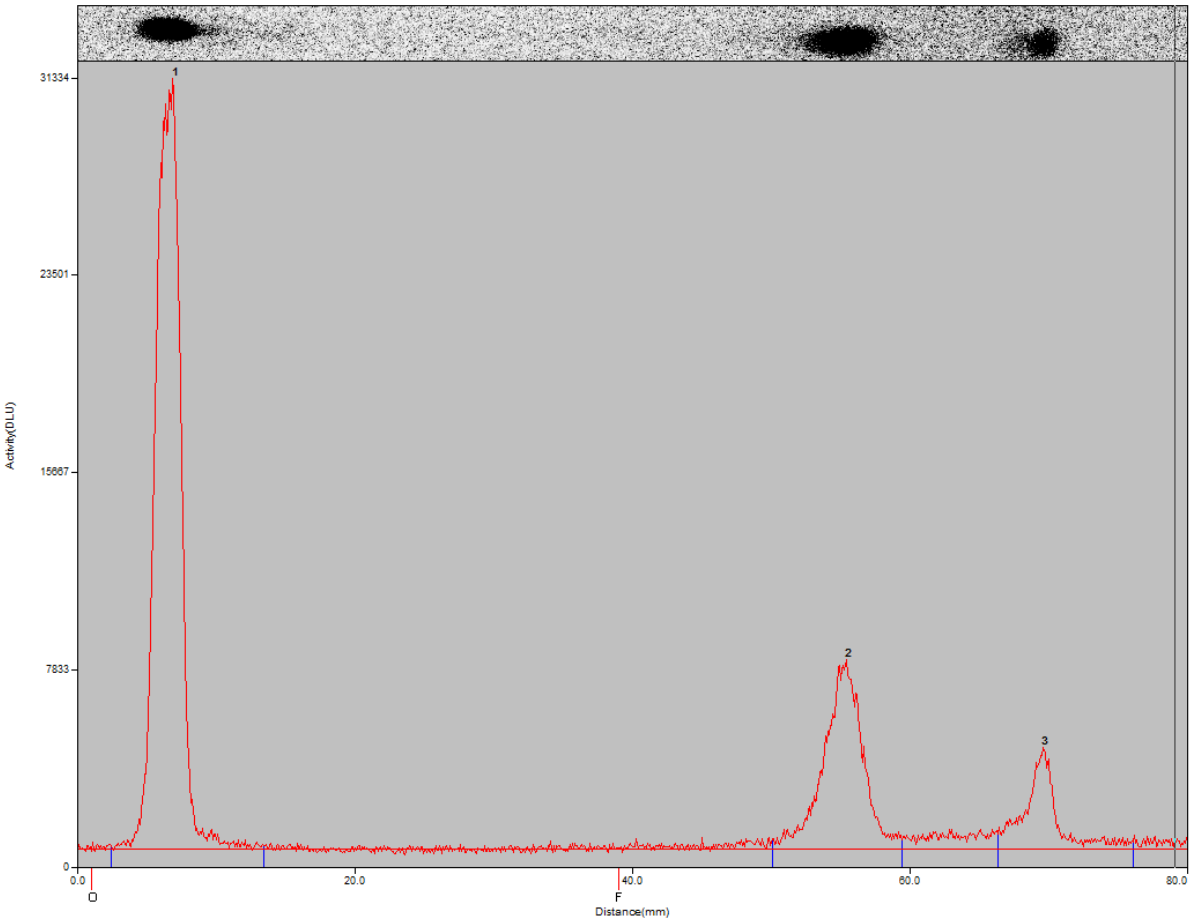

Figure S3.3. RadioTLC peak integration for reaction forming **[^{18}F]PhenESF** at 70°C in 24% RCY (23% by radioHPLC), accompanied by an unknown by-product.

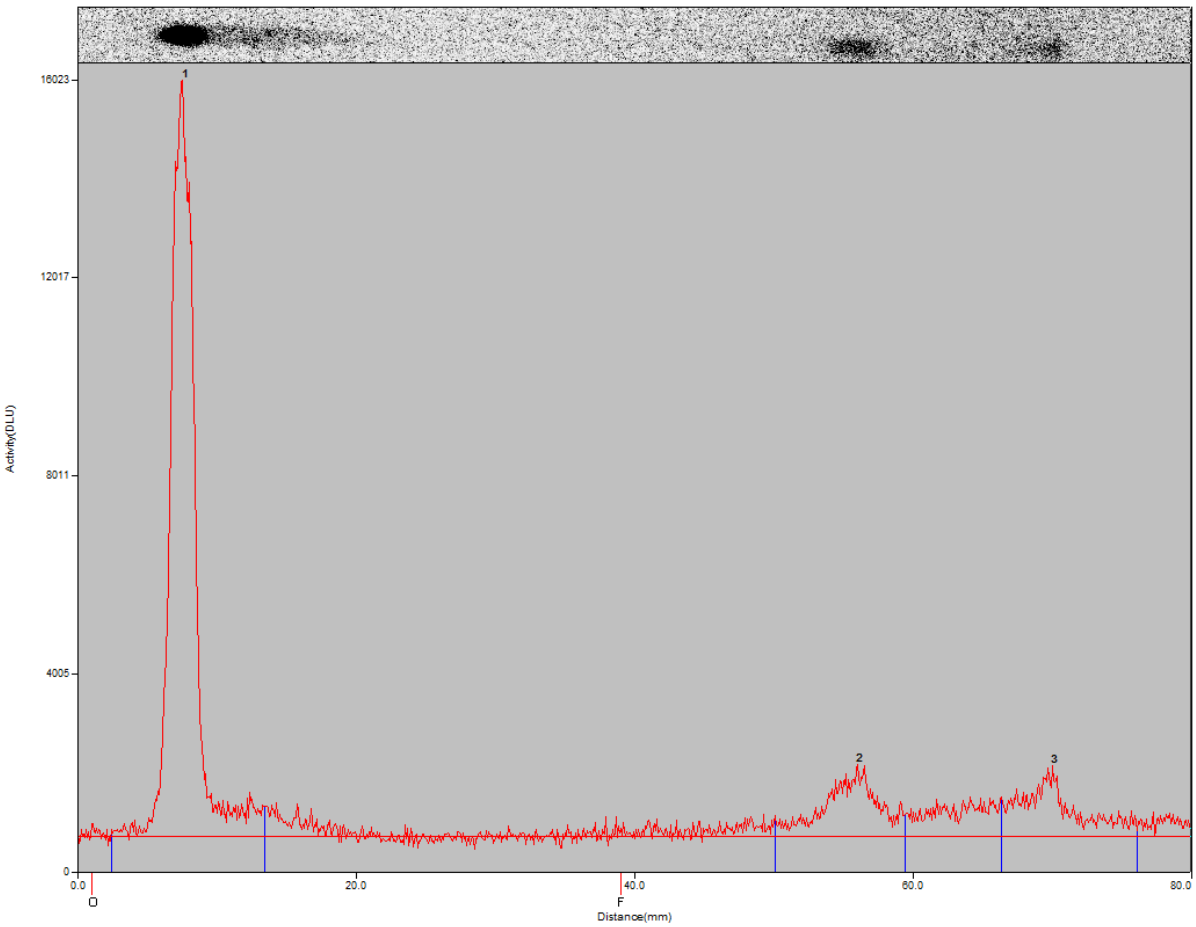

Figure S3.4. RadioTLC peak integration for reaction forming **[^{18}F]PhenESF** at 40°C in 14% RCY (13% by radioHPLC), accompanied by an unknown by-product.

S4. Detailed analysis of the DFT computed Mechanism

The first molecular event is the attack of the lone pair of the amino group on the β carbon of the **ESF**. In the transition state of the attack (**TS_{attack}**) the distance between the nitrogen and the carbon is 1.808 □, with a free energy content of 16.8 kcal/mol. The attack step leads to an intermediate species (**Int**), in which the nitrogen atom is still bound to two hydrogen atoms and it carries a formal positive charge. The negative charge is located to the carbon in β position to the nitrogen. This charge separation leads to the shift of one proton from the nitrogen to the α-carbon, passing through the transition state **TS_{shift}** (N···H = 1.253 □, C···H 1.576 □, ΔE = 22.5 kcal/mol, ΔG = 36.8 kcal/mol). After the proton shift, the structure relaxes to the product of the reaction (**Prod,** ΔE = -26.9 kcal/mol, ΔG = -10.3 kcal/mol).

When the phenanthroline is complexed on the rhenium, the mechanism of the reaction is similar. The transition state of the attack has a higher free energy content (22.2 kcal/mol) and a lower N-C distance (1.754 Å) with respect to the uncoordinated ligand. In order to find a rational for this result, the electronic and geometrical properties of **$PhenNH_2$** and **$RePhenNH_2$** can be compared. The C-N bond is longer in the uncoordinated ligand than in the coordinated one (1.394 and 1.389 Å, respectively), and the lone pair of the nitrogen atom is more occupated in the uncoordinated ligand than in the coordinated one (1.79 and 1.75 e, respectively). This information indicate that the lone pair of the nitrogen is slightly more involved in the double bond C-N, when coordinated, and, therefore, less available for a nucleophilic attack, in agreement with the higher free energy content of **$ReTS_{attack}$** with respect to **TS_{attack}**.

The complex **$RePhenNH_2$** has been analysed also in terms of the Natural Orbitals for the Chemical Valence-Charge Displacement framework.[1–3] According to this framework, the metal-ligand bond is decomposed in different contributions ($\Delta\rho_k$, $k \geq 0$), each of which related to an electronic rearrangement upon the formation of the bond. The rhenium-**$PhenNH_2$** bond can be decomposed in four main contributions. $\Delta\rho_0$ and $\Delta\rho_2$ are related to the σ donation from the nitrogens of the phenanthroline to the metal, whereas $\Delta\rho_1$ and $\Delta\rho_3$ describe the M → **$PhenNH_2$** π back donation. In all of the contributions the ligand is polarized, with a displacement of electronic density toward the metal (positive values of the curves in Figure S4.1).

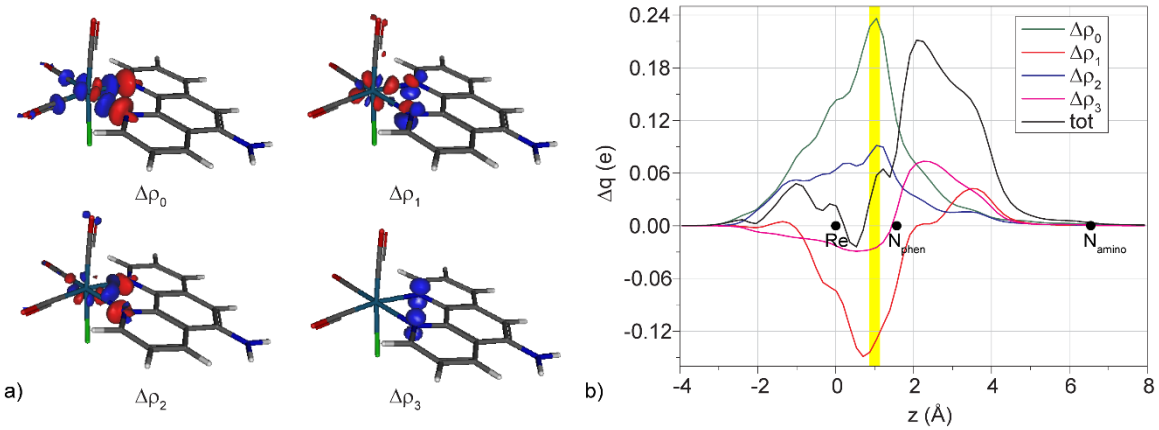

Figure S4.1. (a) Isodensity surfaces (±0.0020 e/au) for the most relevant $\Delta\rho'_k$ (k = 0-3) for complex **RePhenNH$_2$**; (b) Total NOCV-CD curve and its most relevant components for the [ReCl(CO)$_3$] −**PhenNH$_2$** bond. Black dots indicate the *z* position of the atomic nuclei. A yellow vertical band indicates the boundary between the [ReCl(CO)$_3$] and **PhenNH$_2$** fragments.

After the attack, one of the hydrogen atoms moves from the nitrogen to the oxygen of the **ESF**. This can be explained with the same effect of the metal analysed before: indeed, the presence of a positively charged ammonium moiety is disfavoured by the presence of the rhenium, which, as before, attracts electronic density. As a consequence, the amino group and S-OH moieties form, with the positive charge formally delocalized on the sulphur and the oxygen. The negative charge is formally located on the α carbon, as before.

The next molecular event is the proton shift, but the proton is now located on the oxygen, as seen before. The direct shift from the oxygen to the carbon is not possible, therefore the proton has to move back to the nitrogen and then move to the carbon, leading to the geometry **ReTS$_{shift}$**, having a free energy content of 40.8 kcal/mol, also in this case higher than that of **TS$_{shift}$** (36.8 kcal/mol). The presence of the ammonium moiety is likely responsible for this effect, as discussed before. The proton shift leads to the desired product, **Re$_{prod}$**.

The NOCV-CD analysis on **RePhenESF** gives results qualitatively similar to that for **RePhenNH$_2$**, with the difference that in this case the polarization extends up to the sulphur atom (z = 9.3 Å).

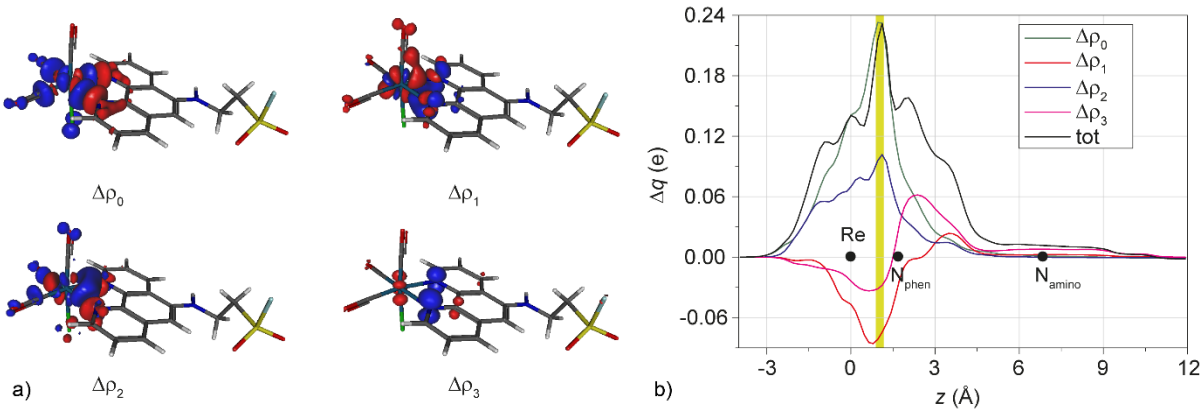

Figure S4.2. (a) Isodensity surfaces (±0.0020 e/au) for the most relevant $\Delta\rho'_k$ (k = 0-3) for complex **RePhenESF**; (b) Total NOCV-CD curve and its most relevant components for the $[ReCl(CO)_3]$ −**PhenESF** bond. Black dots indicate the *z* position of the atomic nuclei. A yellow vertical band indicates the boundary between the $[ReCl(CO)_3]$ and **PhenESF** fragments.

S5. Microfluidic set-up for [^{18}F]ESF production

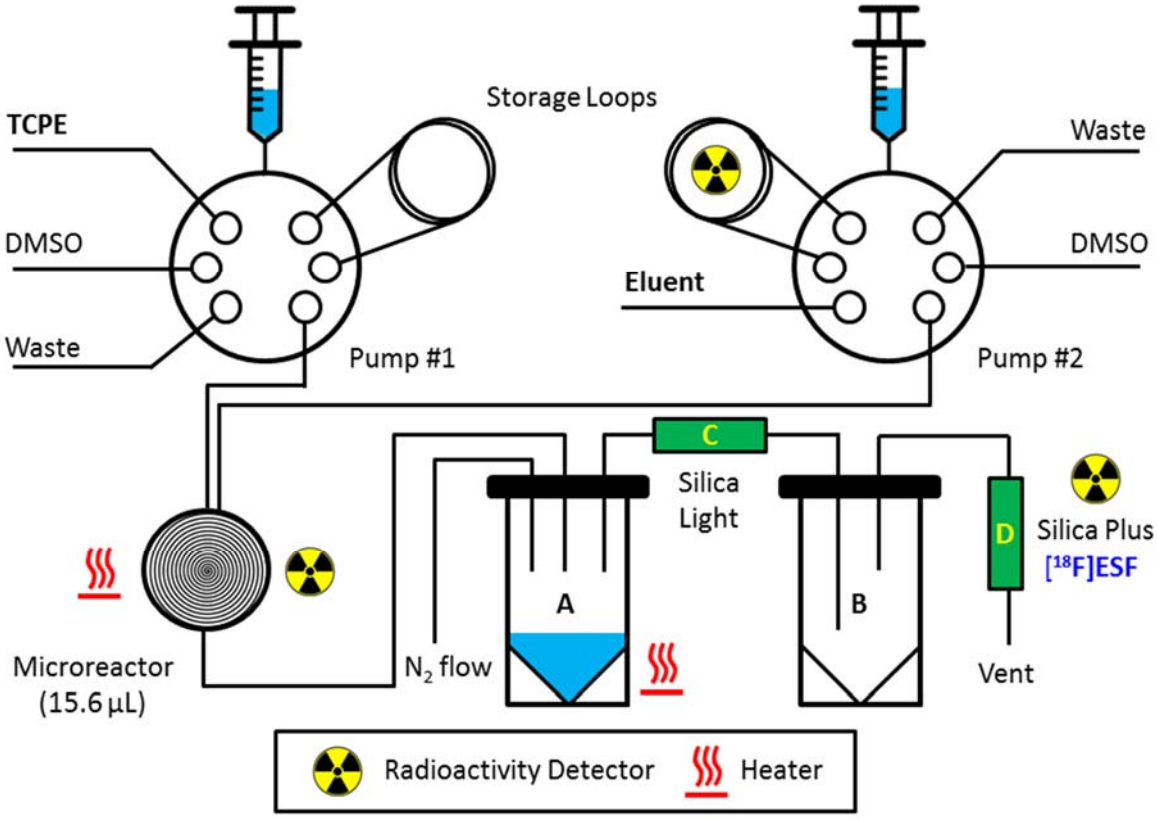

Figure S5.1 Microfluidic set-up used to produce n.c.a. [^{18}F]ESF. The outlet of the microfluidic system is connected to a closed vial (A) heated at 80 °C and pressurized with N_2 gas (0.1 - 0.2 L.min^{-1}). The gaseous effluents from vial A are directed through a silica light SPE cartridge (C) into a second vial (B). The outlet of vial B is connected to a Silica plus SPE cartridge (D) which traps the distilled [^{18}F]ESF.

S6. UV Spectra of Rhenium Complexes

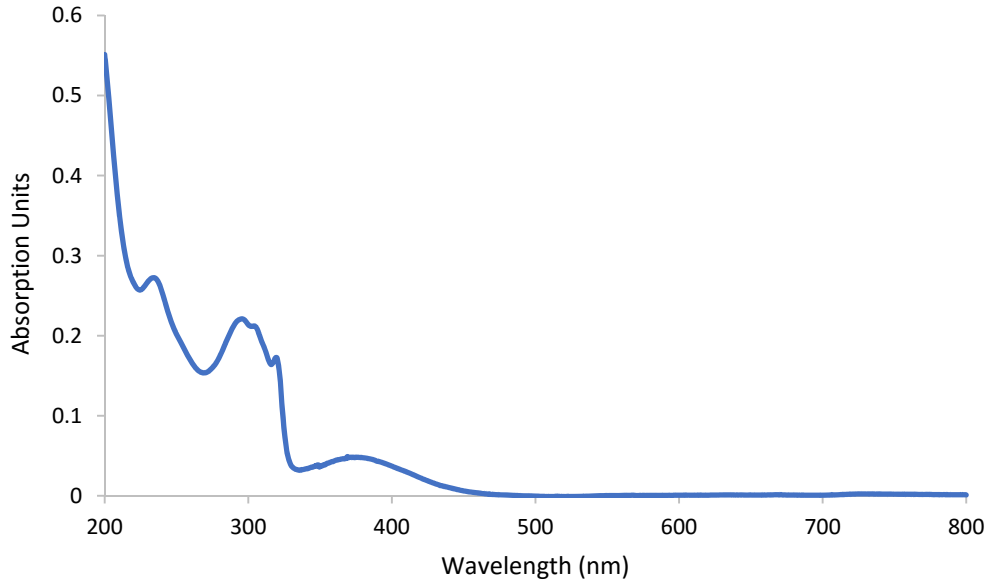

Figure S6.1 UV-Vis absorption spectrum for **RePhenNH$_2$** (2 mg.mL^{-1} in acetonitrile).

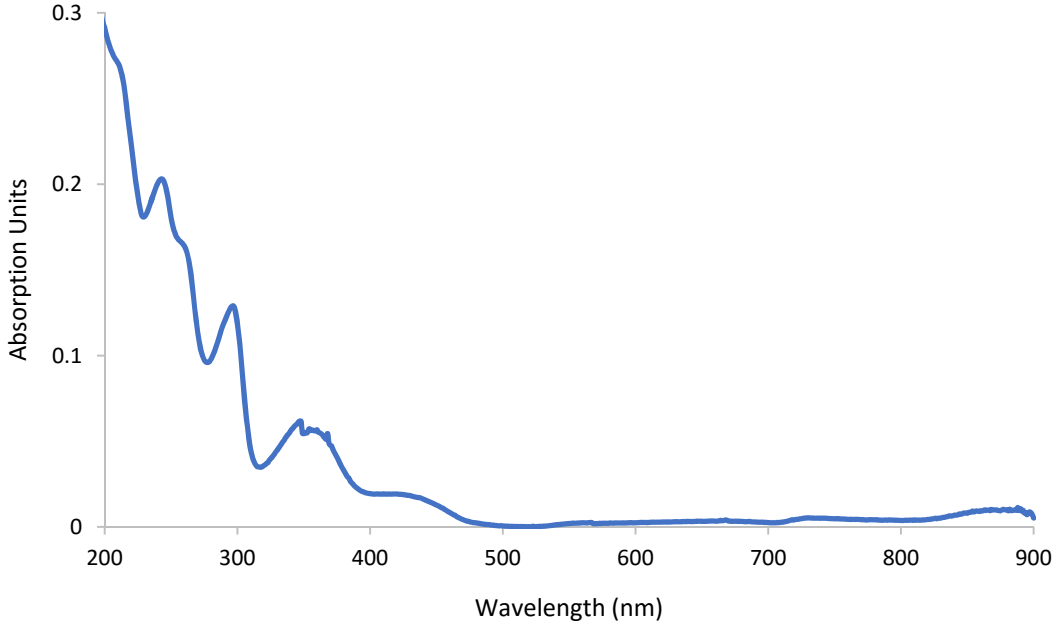

Figure S6.2 UV-Vis absorption spectrum for **RePhenESF** (5 mg.mL^{-1} in acetonitrile).

S7. Photophysical Characterisation Data

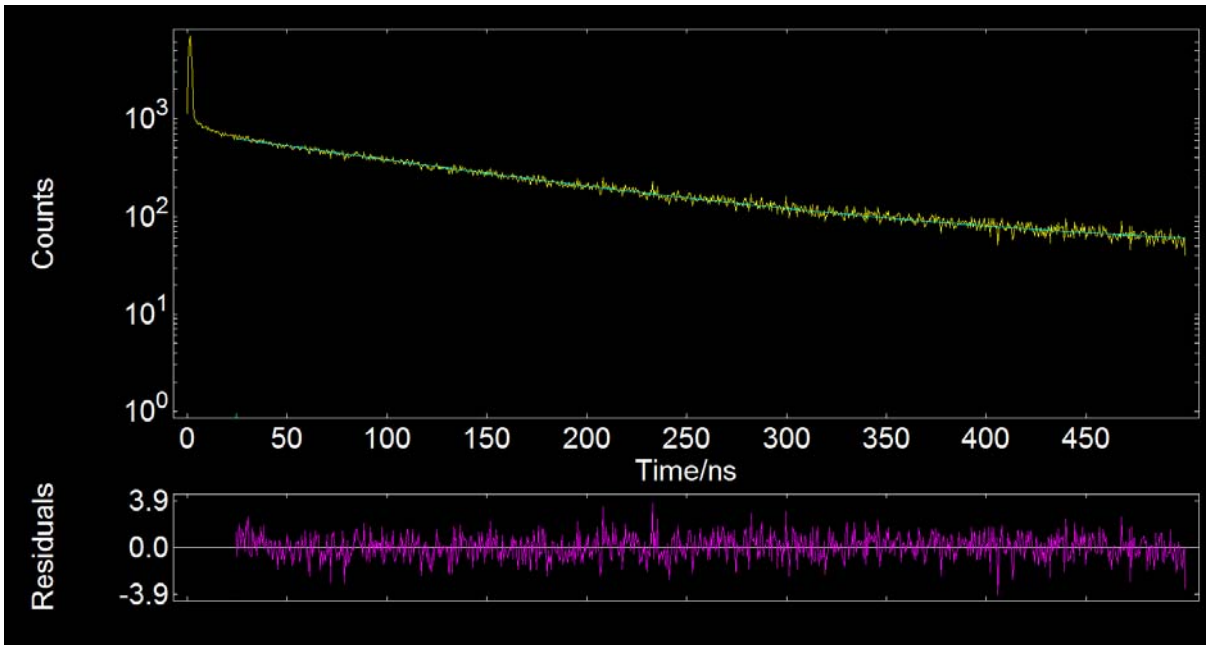

Figure S7.1 Monoexponential decay profile (top) determined for **RePhenESF** in DMSO with weighted residuals (bottom), $\chi^2 = 0.995$.

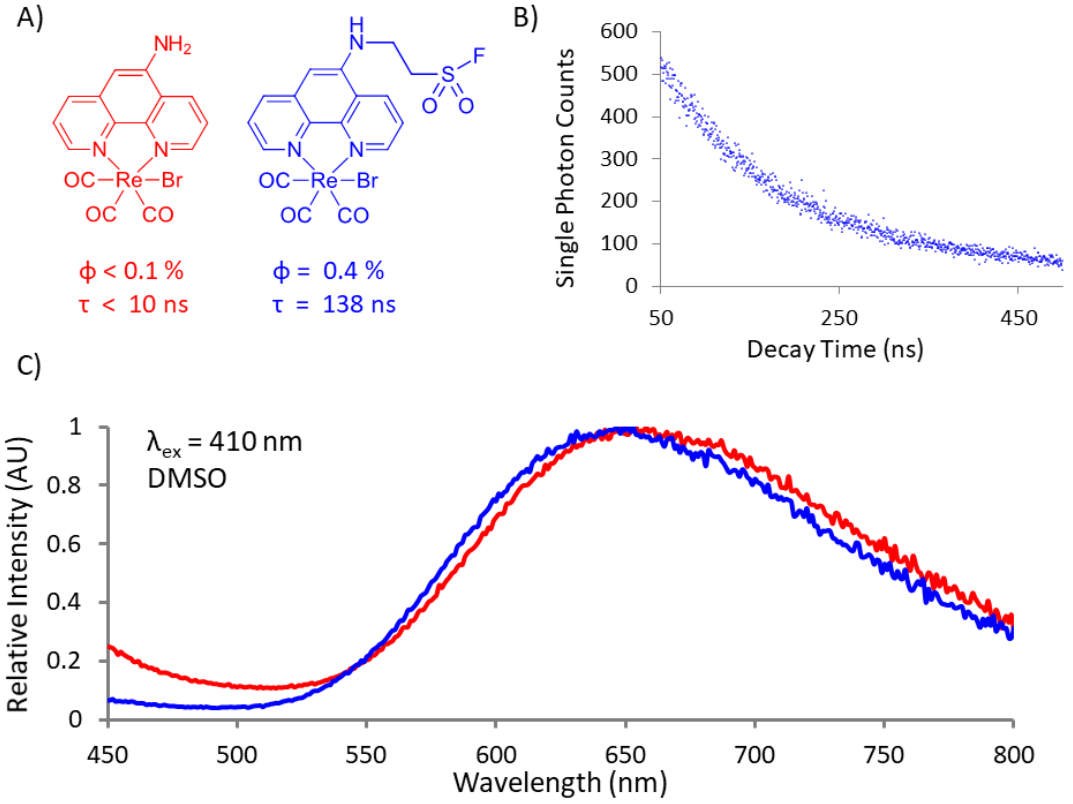

Figure S7.2 A) Quantum yields and lifetimes for **RePhenNH₂** and **RePhenESF**, B) Excited state decay for **RePhenESF** from which the lifetime was determined, C) Normalised emission profiles of **RePhenNH₂** (red) and **RePhenESF** (blue).

S8. References for Supplementary Information

[1] G. Bistoni, S. Rampino, F. Tarantelli, L. Belpassi. *J. Chem. Phys.* **2015**, *142*, 84112.

[2] M. Radon. *Theor. Chem. Acc.* **2008**, *120*, 337-339.

[3] M. Mitoraj, A. Michalak. *J. Mol. Model.* **2007**, *13*, 347-355.